Journal of Materials Chemistry A

ROYAL SOCIETY OF CHEMISTRY

PAPER

View Article Online
View Journal

Cite this: DOI: 10.1039/d4ta04675g

Photo-nanozyme coupling catalyzes glucose oxidation for high-performance enzymatic biofuel cells†

Dandan Hu, [a] Qiwen Su,[a] Yan Gao,[a] Jian-Rong Zhang, *[a] Linlin Wang*[b] and Jun-Jie Zhu *[a]

Glucose biofuel cells (GBFCs) are special energy conversion devices using naturally abundant glucose as fuel. However, achieving high power output and stability remains a challenge in existing GBFCs. In this study, we created a photoelectric coupling nanozyme catalyst of Au/$BiVO_4$ with triple synergistic promotion effects: the surface plasmon resonance of Au significantly broadened the photo-absorption region, enhanced the light absorption intensity, and increased the carrier density of $BiVO_4$; furthermore, the outstanding electron transfer capacity of Au accelerated the photoelectron separation from the vacancies in $BiVO_4$, endowing $BiVO_4$ with excellent photo-corrosion resistance; additionally, the three-dimensional structure of $BiVO_4$ provides abundant sites for Au, remarkably improving the loading and catalytic stability of Au. Consequently, the Au/$BiVO_4$ catalytic GBFC can simultaneously convert solar and chemical energy stored in glucose into electrical energy, providing an extraordinarily high power density and open-circuit voltage (575 μW cm^{-2} and 0.86 V) and working steadily for 20 hours. Altogether, high power output and high stability are achieved in the Au/$BiVO_4$ catalytic GBFC. Thus, this study will significantly propel the development of GBFCs through the innovative application of the photoelectric coupling nanozyme catalytic strategy.

Received 5th July 2024
Accepted 25th August 2024

DOI: 10.1039/d4ta04675g

rsc.li/materials-a

1 Introduction

Enzymatic biofuel cells (EBFCs) are sustainable energy supply devices that utilize biological enzymes as catalysts to convert the chemical energy stored in biological molecules (such as sugars, alcohols, and amines) into electrical energy.[1–3] Thus, EBFCs exhibit high biosecurity, becoming the ideal energy source for implantable medical devices, wearable electronic devices, and *in vivo* biosensors.[4–8] Glucose, particularly abundant in biological systems, possesses a high theoretical energy density of 4430 W h kg^{-1}. Thus, glucose biofuel cells (GBFCs) draw significant attention in the fields of energy, healthcare, and biosensors.[9–12] However, the high power output and high stability have yet to be realized simultaneously in the reported GBFCs.[13] The main reasons are that the natural enzymes are fragile and show sluggish extra-molecular electron transfer rates.

Nanozymes, nanomaterials with enzyme-like activities, are ideal substitutes for natural enzymes in electrocatalysis due to their enhanced stability, robust catalysis, adjustable microstructure, and more efficient electron transfer.[14,15] According to their material composition, nanozymes can be divided into non-precious and precious metal-based nanozymes.[16] The former is cost-effective, but they only exhibit high catalytic performance under strong alkaline or acidic conditions.[17] The latter is costly, but their catalytic performance is superior and pH-independent; thus, their catalytic value far outweighs their cost. Among precious metal-based nanozymes, Au nanomaterials exhibit a catalytic mechanism similar to natural enzymes like glucose oxidase (GOD or GOx).[18] In light of this, a series of Au-based nanozyme catalytic GBFCs were developed. Their lifetime could be extended to 15 days, but the power output was less than 144.7 μW cm^{-2}.[19–21] This is primarily attributed to the unsatisfactory catalytic activity and efficiency of the reported nanozymes.

Differing from electro-catalysts, photo-electro-catalysts harness solar and electrical energy to drive glucose oxidation, significantly reducing energy consumption and enhancing catalytic efficiency.[22–25] However, the application of photo-electro-catalysts in GBFCs still faces formidable challenges: the electron generated by photoexcitation is easy to accumulate on the catalyst surface, resulting in photo-corrosion, which severely shortens the lifetime and reduces the catalytic activity

[a]State Key Laboratory of Analytical Chemistry for Life Science, School of Chemistry and Chemical Engineering, Nanjing University, Nanjing 210023, P. R. China. E-mail: jrzhang@nju.edu.cn; jjzhu@nju.edu.cn

[b]Shaanxi Key Laboratory of Chemical Additives for Industry, College of Chemistry and Chemical Engineering, Shaanxi University of Science and Technology, Xi'an 710021, China. E-mail: wanglinlin@sust.edu.cn

† Electronic supplementary information (ESI) available: Materials and methods, experimental details and additional experimental data. See DOI: https://doi.org/10.1039/d4ta04675g

of the photo-electro-catalysts;[26] moreover, the catalytic selectivity of these catalysts is poor.[10,27,28] Considering that most of the glucose oxidase-like nanozymes are good conductors of electrons and have a specific affinity for glucose, therefore, the integration of nanozymes with photoelectric nanomaterials will make a breakthrough in developing GBFCs with high power output and longevity.

In this study, we have fabricated a photoelectric coupling nanozyme catalyst of Au/$BiVO_4$ as the anodic catalyst of the GBFC. As depicted in Fig. 1, Au/$BiVO_4$ exhibited triple synergistic promotion effects beyond simple combinations. Firstly, the outstanding electron conductivity of Au accelerated the photoelectron transfer from the vacancies of $BiVO_4$, endowing $BiVO_4$ with excellent photo-corrosion resistance. More importantly, we conducted a dark-field microscopic imaging test and discovered that the nanozyme of Au had a surface plasmon resonance effect, significantly broadening the photo-absorption region, enhancing the light absorption intensity, and increasing the carrier density of $BiVO_4$, eventually improving the catalytic activity of $BiVO_4$. It's also worth noting that the three-dimensional structure of $BiVO_4$ provided abundant location sites for Au, which could enhance Au loadings and catalytic stability. The Au covered on the $BiVO_4$ surface, in turn, increased the glucose concentration at the $BiVO_4$ interface due to the high affinity of Au for glucose. Consequently, coupling with the bilirubin oxidase (BOD) biocathode, the Au/$BiVO_4$ catalytic GBFC could simultaneously convert the solar energy and chemical energy stored in glucose into electrical energy and offered an extraordinarily high power output density of 575 μW cm^{-2}, 72-times higher than that of the GOD-catalyzed GBFC. And the lifetime of the GBFC was prolonged to 20 hours. Altogether, both the high power output and high stability were realized in the Au/$BiVO_4$ catalytic GBFC.

2 Experimental section

2.1. Synthesis of the $BiVO_4$ electrode

Firstly, the precursor electrode, BiOI electrode, was prepared by an *in situ* electrochemical deposition method in a three electrode system, in which a clean FTO (geometric area is 1.0 × 1.0 cm^2) substrate, an Ag/AgCl (4 M KCl) electrode and a platinum wire electrode were used as the working electrode (WE), the reference electrode (RE) and the counter electrode (CE), respectively. The electrolyte was prepared as follows: 0.4 M KI and 0.04 M bismuth nitrate were dissolved in nitric acid solution (pH 1.7, 50 mL) to obtain an orange transparent solution. The above solution was then mixed with 0.23 M *p*-benzoquinone (alcohol, 20 mL). Electrolyzing the FTO electrode in the above electrolyte at −0.1 V for 60–360 s yielded the BiOI electrode.[29] Then, 200 μL of 0.2 M vanadium acetylacetonate (dissolved in DMSO) was added dropwise to the BiOI electrode and dried at 60 °C. The dried electrode was calcined at 450 °C in a muffle furnace for 2 hours at a heating rate of 2 °C min^{-1} and then cooled down to room temperature, followed by a 30 min rinse with 1 M NaOH to remove excess V_2O_5, and a rinse with water to remove excess NaOH. The bright yellow bismuth vanadate electrodes were obtained after drying in air.

2.2. Synthesis of the Au/$BiVO_4$ hybrid anode

The Au/$BiVO_4$ anode was synthesized through electrolyzing the obtained $BiVO_4$ electrode in an anaerobic $HAuCl_4 \cdot 4H_2O$ solution (0.6 mM). The electrochemical deposition process was implemented by cyclic voltammetry for two cycles in the voltage range from −0.7 to −0.1 V *vs.* Ag/AgCl with a scan rate of 0.001 V s^{-1}.

2.3. Synthesis of the GOD/SWCNT/CC bioanode

To enhance the electron transfer rate between the GOD and the electrode, the single-walled carbon nanotube (SWCNT) film was fabricated according to the literature[4] (a detailed preparation process is provided in the ESI†). To obtain the SWCNT/CC (carbon cloth) substrate, the previously prepared SWCNT film was cut into an area of 0.6 × 0.6 cm^2 and then fixed to the carbon cloth substrate by π–π force using pressure. Subsequently, the SWCNT/CC substrate electrode was placed into 1 mM 1-pyrene butanoic acid succinimidyl ester (PBSE) solution for 30 min to create sites for GOD immobilization, followed by rinsing with deionized water to eliminate residual PBSE.[30] Finally, the functionalized SWCNT/CC electrode was incubated with GOD (4 mg mL^{-1}, 100 μL) for 12 hours, followed by rinsing

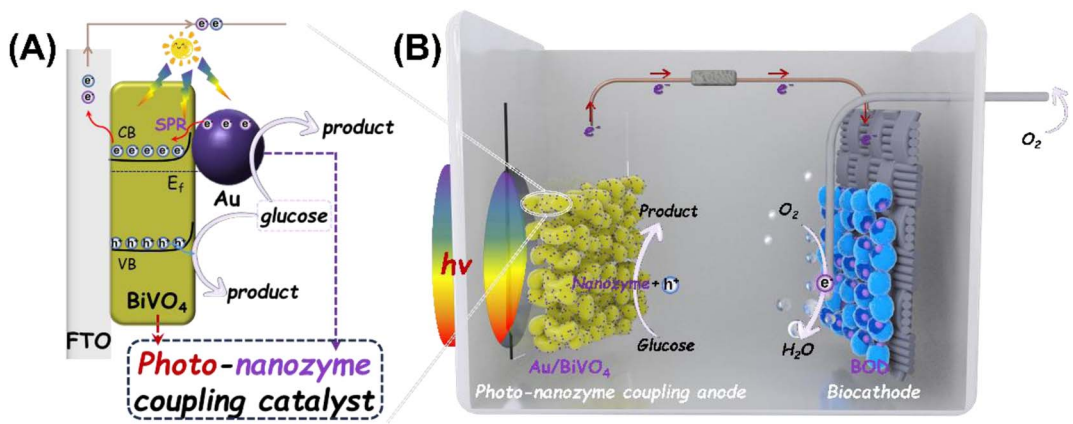

Fig. 1 Schematic illustrating (A) the catalytic mechanism diagram of the Au/$BiVO_4$ photo-nanozyme coupled catalyst for glucose and (B) the design outline of our innovative glucose/oxygen biofuel cell (GBFC).

with water to obtain the bioanode of GOD/SWCNT/CC. The bioanode was stored at 4 °C for further use.

2.4. Synthesis of the BOD/SWCNT/CC biocathode

100 μL of BOD (8 mg mL^{-1}) was dropped onto the SWCNT/CC electrode and reacted for 12 hours to obtain the BOD/SWCNT/CC biocathode and stored at 4 °C for future use.

2.5. Preparation of the membrane-less GBFC

The Au/$BiVO_4$ photo-nanozyme anode and BOD biocathode were placed in a square, quartz electrolytic cell with a 5 × 5 × 5 cm^3 volume. The anode and cathode were positioned opposite each other to form a single chamber GBFC, with a distance of 3 cm between them. The GBFC was then operated in an O_2-saturated phosphate buffer (PB, 0.2 M, pH 7.4) with different concentrations of glucose, and the polarization curves were recorded using a CHI 660 D workstation with a scan rate of 1 mV s^{-1}.

3 Results and discussion

3.1. Morphology and structure characterization of Au/$BiVO_4$

As illustrated in Fig. 2A, the BiOI nanosheets formed *in situ* on the FTO surface by electrodeposition. After calcining the BiOI nanosheets with vanadyl acetylacetonate, a layer of uniform $BiVO_4$ with a 800 μm thick and porous nano-worm three-dimensional structure was fabricated (Fig. 2B). A more detailed test of TEM revealed that the $BiVO_4$ layer was composed of nanoparticles (Fig. 2C). What's more, the particle size increased with the increase of BiOI precursor electrodeposition time, and the $BiVO_4$ fabricated from the BiOI with an electrodeposition time of 60 s exhibited higher catalytic activity for glucose oxidation (Fig. S1 and S2†). However, the highest current density for glucose oxidation catalyzed by $BiVO_4$ was only 1.61 mA cm^{-2} (at 0.5 V), and the most probable reason was the poor electron conductivity of semiconductor $BiVO_4$. Given this, we attempted to decorate the $BiVO_4$ with Au nanoparticles (AuNPs), a kind of highly conductive nanozyme, constructing a photoelectric coupling nanozyme catalyst (Au/$BiVO_4$). As revealed in Fig. 2D–F, the AuNPs with ~10 nm particle size uniformly grew on the $BiVO_4$ surface. The XRD results in Fig. 2G further confirmed the successful transition from BiOI (JCPDS: 10-0445) to $BiVO_4$ (JCPDS: 14-0688), and the AuNPs with the most exposed crystal face of Au (111) were formed on the $BiVO_4$ surface (Fig. 2H). Research has proven that the Au (111) crystal face plays a dominant role in Au nanozyme catalytic glucose oxidation.[31] Therefore, it's reasonable that the Au can not only

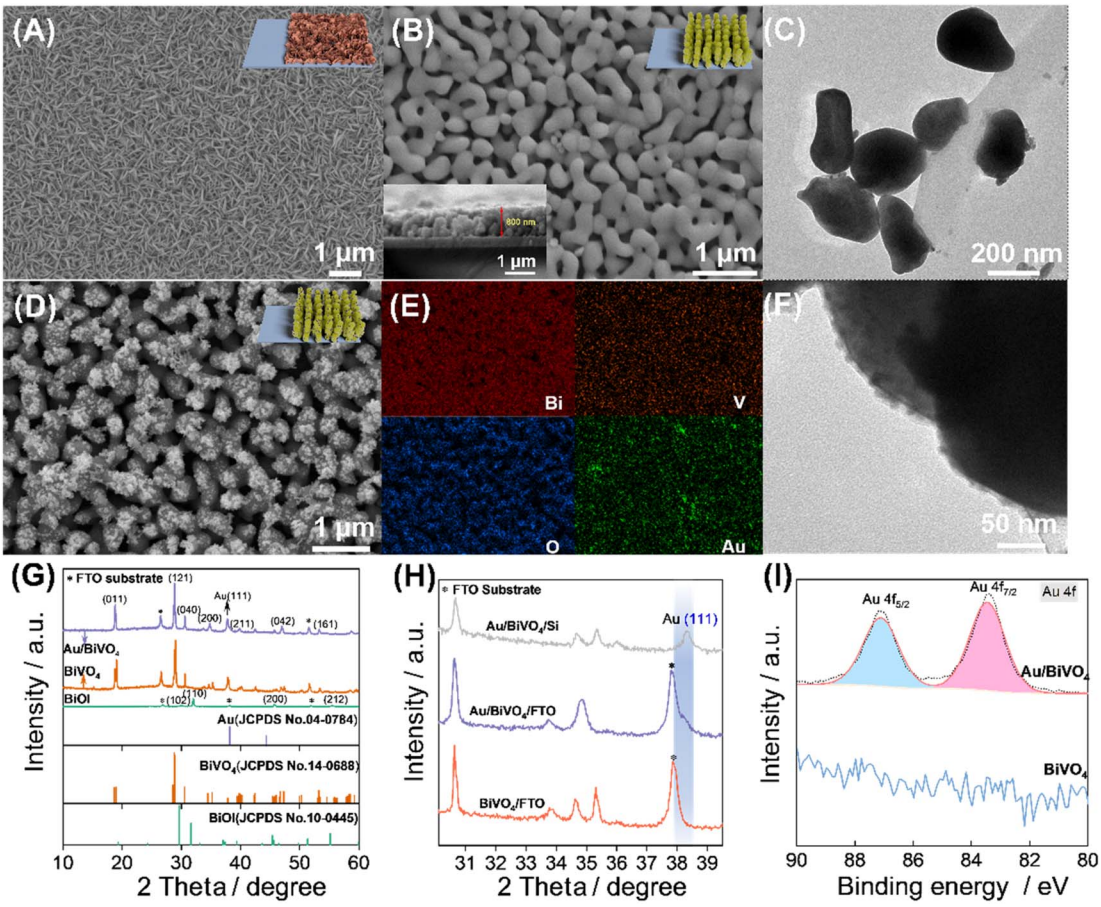

Fig. 2 Fabrication and characterization of the $BiVO_4$ with AuNPs. SEM images of (A) BiOI and (B) $BiVO_4$ (inset: cross-sectional view SEM images). (C) TEM images of $BiVO_4$. (D) SEM images, (E) mapping images, and (F) TEM images of Au/$BiVO_4$. (G) XRD patterns for BiOI, $BiVO_4$, and Au/$BiVO_4$. (H) XRD detailed patterns of $BiVO_4$/FTO, Au/$BiVO_4$/FTO, and Au/$BiVO_4$/Si. (I) High-resolution XPS spectra of Au 4f for Au/$BiVO_4$.

accelerate the electron transfer rate of $BiVO_4$ but also perform a synergistic catalysis. It's worth noting that, as the XPS analysis revealed, the binding energy of Au 4f showed a slight reduction compared to naked Au (Fig. 2I and S3†), demonstrating the strong electron interaction between Au and $BiVO_4$, which is highly helpful for the photoelectric coupling catalysis.

3.2. Photoelectric properties of Au/$BiVO_4$

As a kind of photo-electro-catalyst, a remarkable light absorption ability is the requisite for superior catalysis. The light absorption properties of the $BiVO_4$ and Au/$BiVO_4$ were explored using UV-vis diffuse reflectance spectra (DRS), and the results are presented in Fig. 3A. The $BiVO_4$ with an absorption edge at 500 nm and its band gap is determined to be 2.45 eV from the Tauc diagram (Fig. S4A†). Intriguingly, compared to pristine $BiVO_4$, the light absorption intensity of Au/$BiVO_4$ significantly increased, and the absorption range is slightly red-shifted (~510 nm), corresponding to a narrow band gap of 2.36 eV (Fig. S4A†). To get more facts about the photoelectric properties of Au/$BiVO_4$, Mott–Schottky (M–S) tests were conducted. The carrier densities (N_d) of $BiVO_4$ and Au/$BiVO_4$ can be calculated from the Mott–Schottky (M–S) slope of Fig. 3B (detailed calculations can be found in ESI Section 1.4). The obtained N_d value for Au/$BiVO_4$, which is 8.7×10^{17} cm^{-3}, exhibits enhancement compared to the pristine $BiVO_4$ value of 5.3×10^{17} cm^{-3}. This observation demonstrates that both the carrier concentration and carrier mobilization rate are enhanced by the composite of $BiVO_4$ with Au. Also of note, the flat band potential (E_{fb}) of $BiVO_4$ and Au/$BiVO_4$ calculated from the M–S curves was −0.39 V and −0.59 V *vs.* Ag/AgCl (0.24 V and 0.05 V *vs.* RHE), respectively. Therefore, the corresponding valence bands of $BiVO_4$ and Au/$BiVO_4$ are 2.49 V and 2.21 V, respectively (a detailed calculation process is provided in the ESI†). Given that the theoretical glucose oxidation potential is 0.05 V,[32] both $BiVO_4$ and Au/$BiVO_4$ have the potential to catalyze glucose oxidation. More importantly, compared with $BiVO_4$, the valence bands of Au/$BiVO_4$ exhibited ~0.2 V up-shift, being highly helpful in suppressing the side reaction of water oxidation.[33] Altogether, we could preliminarily conclude that Au/$BiVO_4$ possesses superior photocatalytic performance for glucose oxidation due to the enhanced carrier density, carrier migration rate, and favorable valence bands.

To further study the photoelectric enhancement mechanism of Au/$BiVO_4$, we carried out electrochemical impedance spectroscopy (EIS) and dark-field microscopic imaging tests. The EIS results revealed that the charge transfer resistance of Au/$BiVO_4$ was about 340 Ω, much smaller than the charge transfer resistance value of 606 Ω for $BiVO_4$ (Fig. 3C). This acceleration effect on electron transfer was mainly due to the outstanding electron conductivity of Au and was highly conducive to photoelectron-vacancy separation to improve the photo-corrosion resistance of $BiVO_4$. Moreover, the green scattered light (at 560 nm) of 10 nm Au nanoparticles was clearly observed in the dark-field microscopic image (Fig. 3D); this result is consistent with the SPR peak observed for Au in Fig. 3A. After coupling with $BiVO_4$, the scattered light of Au showed a slight redshift (at 597 nm) (Fig. 3E and F), confirming the surface plasmon resonance of Au. Due to the surface plasmon resonance, the Au could generate hot electrons, which can be injected into the conduction band of $BiVO_4$, finally increasing the carrier density of Au/

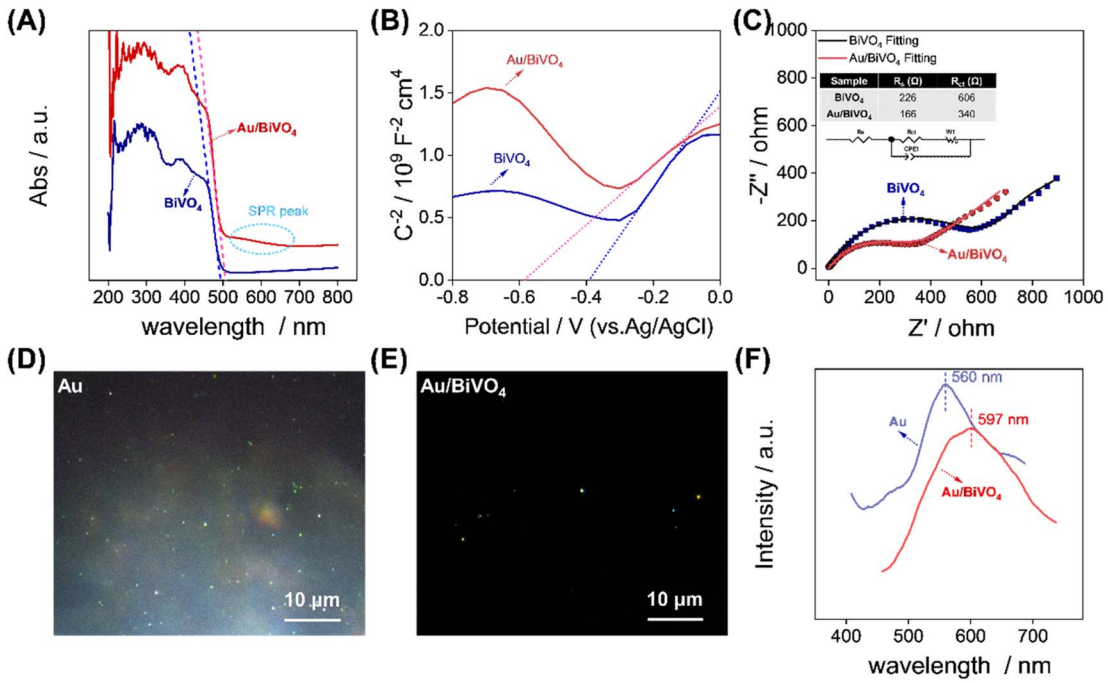

Fig. 3 (A) UV-vis diffusion absorption spectra and (B) Mott–Schottky curves for both $BiVO_4$ and Au/$BiVO_4$. (C) Electrochemical impedance spectroscopy (EIS) curves for the Au/$BiVO_4$ and $BiVO_4$ electrodes. Dark field microscopy images of (D) individual gold particles and (E) Au/$BiVO_4$ in phosphate buffer solution. (F) Surface plasmon resonance (SPR) scattering spectra of Au and Au/$BiVO_4$.

$BiVO_4$.[34] Meanwhile, enhanced electron density in the conduction band of $BiVO_4$ elevates its Fermi energy level, potentially resulting in a negative shift in the flat-band potential. The negative shift of the flat band potential leads to the reduction of the valence band of the catalyst, which inhibits the oxidation of water. Ultimately, the oxidation of glucose by Au/$BiVO_4$ was enhanced. The above results suggested that Au/$BiVO_4$ will be a superior photoelectrocatalyst for glucose oxidation.

3.3. Photoelectrocatalytic performances of Au/$BiVO_4$

A comparative study of the photoelectrocatalytic activities of Au, $BiVO_4$, and Au $BiVO_4$ was examined *via* linear sweep voltammetry (LSV). As shown in Fig. 4A, under dark conditions, the glucose oxidation current density on the Au electrode was the highest (for Au, $BiVO_4$, and Au/$BiVO_4$, the values are 0.58 mA cm^{-2}, 0.09 mA cm^{-2} and 0.19 mA cm^{-2} at 0.5 V, respectively), confirming the outstanding electro-catalytic activity of nanozyme Au for glucose oxidation. Irradiating with visible light, the glucose oxidation current density slightly increased on the Au electrode, while in cases of $BiVO_4$ and Au/$BiVO_4$ electrodes, the current density obviously increased to 1.6 mA cm^{-2} and 4.2 mA cm^{-2}, and the onset potential negatively shifted to −0.23 V and −0.42 V. These results lead to two conclusions: Au and $BiVO_4$ showed high electro-catalytic and photo-electro-catalytic activities for glucose oxidation. What's more, the photo-electro-catalytic activity showed a 1.6-fold increase after a combination of these two materials, indicating the synergistic catalysis between the Au and $BiVO_4$. This conclusion was further confirmed by the glucose oxidation rate, which was only 35% or 60% in a 6-hour glucose oxidation process catalyzed by $BiVO_4$ or Au but over 90% in the process catalyzed by Au/$BiVO_4$ (Fig. S5B†).

As we observed the valence band potential of Au/$BiVO_4$ (2.21 V) is able to oxidize water (1.23 V) and glucose (0.05 V) in the electrolyte, and the catalytic selectivity directly affects the energy efficiency converted from glucose. In view of this, the catalytic current density on the Au/$BiVO_4$ electrode and the O_2 concentration in the electrolyte generated from water oxidation were investigated. The results in Fig. 4B revealed that the catalytic current density on the Au/$BiVO_4$ electrode increased with the increase of glucose concentration. In contrast, the O_2 concentration decreased, indicating that the glucose oxidation took precedence over water oxidation on the Au/$BiVO_4$ electrode. It is especially noteworthy that the upper limit concentration of glucose in Au/$BiVO_4$ that could efficiently catalyze was as high as 800 mM, and the current density reached 5.6 mA cm^{-2} at 1.23 V *vs.* RHE, higher than the maximum value reported so far (Table S1 and Fig. S6†). This promoted catalytic performance was mainly from the synergistic catalysis between the Au and $BiVO_4$.

3.4. Performance of the Au/$BiVO_4$ catalyzed GBFC

Finally, we assembled a membrane-less GBFC using the Au/$BiVO_4$ and the bilirubin oxidase/single-walled carbon nanotubes (BOD/SWCNTs) as the anodic and cathodic catalysts, respectively, and investigated further the cell's performance. The performance of the BOD/SWCNTs cathode was first studied. As depicted in Fig. S7†, the onset potential for the BOD/SWCNTs cathode was 0.51 V (*vs.* Ag/AgCl), and the current density at 0.0 V reached −1.79 mA cm^{-2}, which was higher than that for Au/$BiVO_4$ at 0.0 V (0.13 mA cm^{-2}), demonstrating that the BOD/SWCNTs will not be the determining factor of GBFC's performance. For the illuminated GBFC, its open-circuit voltage and power density increased with increasing glucose concentration and reached the high-threshold (0.86 V and 575 μW cm^{-2}) when the glucose concentration increased to 800 mM (Fig. 5A and S8†). This GBFC performance trend was highly consistent with that of the Au/$BiVO_4$ anode, further confirming that the GBFC performance was directly determined by the anodic performance. What's more, the power density of the Au/$BiVO_4$ catalyzed GBFC was up to 575 μW cm^{-2}, which was 72-times, 52-times and 3.3-times higher than that of the GBFC catalyzed by the natural enzyme of GOD, nanozyme of Au and $BiVO_4$, respectively (Fig. 5B). More importantly, compared with

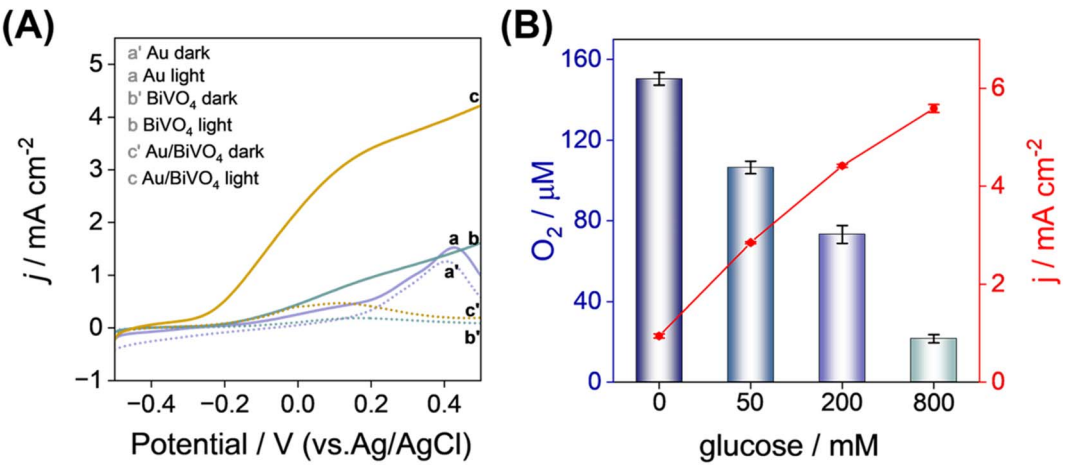

Fig. 4 (A) LSVs curves for the Au, $BiVO_4$, and Au/$BiVO_4$ electrodes in 0.2 M phosphate buffer (pH 7.4) with a glucose concentration of 200 mM, both with or without visible-light irradiation (λ > 420 nm). (B) The dissolved O_2 concentration in the electrolytes and the corresponding current density were measured for various glucose concentrations at 1.23 V *vs.* RHE.

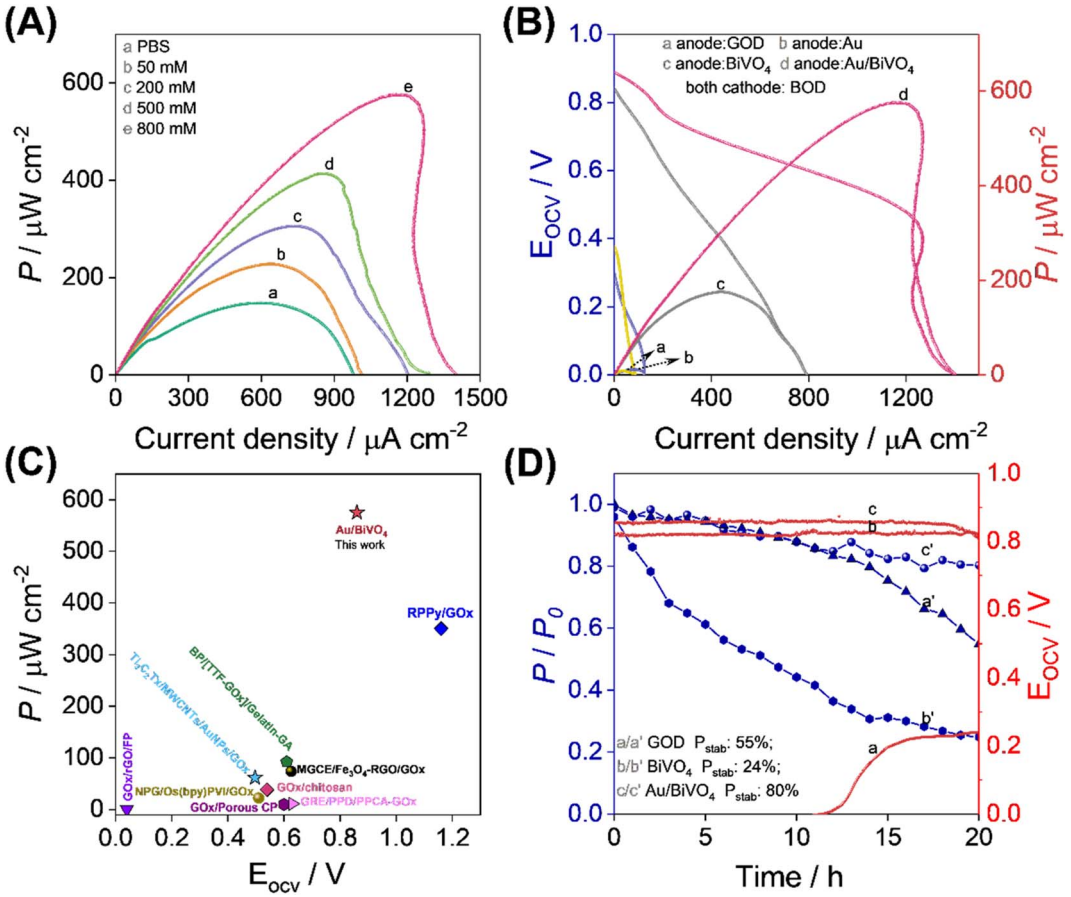

Fig. 5 (A) The power densities of the GBFC corresponding to glucose concentrations of 0, 50, 200, 500, and 800 mM. The scan rate used was 1 mV s^{-1}. (B) Polarization curves and power densities of only enzyme-catalyzed (anode: GOD or Au, cathode: BOD), only photocatalyzed (anode: $BiVO_4$, cathode: BOD), and photo-nanozyme-coupled catalyzed (anode: Au/$BiVO_4$, cathode: BOD) in the GBFC. (C) Performance comparison of photo-nanozyme-based GBFCs constructed in this work and using a natural enzyme GOx as an anode. (D) The stability of discharge and E_{ocv} were evaluated for GBFCs assembled with GOD, $BiVO_4$, or Au/$BiVO_4$ as the anode and BOD as the cathode.

the reported GBFCs constructed either with the natural enzyme GOx as the anode or with photoelectric materials as the anode, the advantage of our anode constructed with photo-nanozyme coupled hybridized materials is the most obvious (Fig. 5C, see detailed comparison in ESI Tables 2 and 3†). It's also worth noting that, compared to the GBFC under dark conditions, the maximum power density of the illuminated GBFC increased by 63 times (Fig. S9B†). Altogether, the optimal power density output was realized in the Au/$BiVO_4$ catalyzed GBFC due to the SPR-mediated synergistic photo-electro-catalysis.

Additionally, we further investigated the GBFC's working stability. As depicted in Fig. 5D, for the Au/$BiVO_4$ catalyzed GBFC, its open-circuit voltage remained so stable at 0.86 V that no remarkable decline was observed within a long term of 20 hours, and its maximum power output only decreased by 20%. Following 20 hours of GBFC discharge, we have observed that the AuNPs were aggregated on the Au/$BiVO_4$ electrode, and the crystal face of Au (111) showed a slight increase (Fig. S10†). Such structural changes may be the key factor in the decay of the GBFC discharge stability. Therefore, enhancing the interfacial bonding strength between AuNPs and $BiVO_4$ will be an effective way to further improve the stability of GBFC, whereas, in cases of natural GOD or $BiVO_4$, the open-circuit voltage dropped dramatically from 0.24 V to 0.02 or 0.82 to 0.80 V at 20 hours; in particular, their maximum power density output dramatically decreased by 45% and 76% after discharge for 20 hours. Such favorable working stability for Au/$BiVO_4$ was attributed to the fact revealed in Fig. 3C that the outstanding electron conductivity of nanozyme Au could accelerate the photoelectron-vacancy separation, improving the photo-corrosion resistance of $BiVO_4$.

4 Conclusions

In summary, we have developed the first GBFC, which had both high power output and a long lifetime, by creating a photoelectric coupling enzyme catalyst of Au/$BiVO_4$. This catalyst could simultaneously convert the solar energy and the chemical energy stored in glucose to electrical energy, favoring increased energy conversion efficiency. Also, the surface plasmon resonance and high electron conductivity of nanozyme Au could increase the carrier density and the photo-corrosion resistance of the $BiVO_4$, respectively. The porous nano-worm $BiVO_4$ could, in turn, improve the loadings and catalytic stability of nanozyme Au. Benefitting from the above synergistic promotion

effects, Au/$BiVO_4$ exhibited highly stable catalytic activity for glucose. Consequently, the GBFC equipped with the Au/$BiVO_4$ anode offered an extraordinarily high power density output of 575 μW cm^{-2}, 72-times and 52-times higher than that of the GBFC catalyzed by GOD and Au, respectively. In the meantime, the open-circuit voltage could remain stable at a high value of 0.86 V for a long period of 20 hours. This study achieves a breakthrough in the field of biofuel cells by creating a new photo-nanozyme coupling strategy with multiple synergistic promotion effects and will renovate the practical application of biofuel cells.

Data availability

The data supporting this article have been included as part of the Experimental section and ESI.†

Author contributions

Dandan Hu: conceptualization, methodology, data curation, writing original draft. Qiwen Su: methodology, formal analysis. Yan Gao: methodology. Jian-Rong Zhang: review & editing, funding acquisition. Linlin Wang: visualization, writing – review & editing, funding acquisition. Jun-Jie Zhu: review & editing.

Conflicts of interest

The authors report no declarations of interest.

Acknowledgements

We gratefully acknowledge the National Natural Science Foundation of China (22374067 and 22004060).

Notes and references

1 X. Xiao, H. Xia, R. Wu, L. Bai, L. Yan, E. Magner, S. Cosnier, E. Lojou, Z. Zhu and A. Liu, *Chem. Rev.*, 2019, **119**, 9509–9558.
2 H. Chen, F. Dong and S. D. Minteer, *Nat. Catal.*, 2020, **3**, 225–244.
3 L. Wang, J.-R. Zhang, X. Wu and J.-J. Zhu, *TrAC, Trends Anal. Chem.*, 2022, **146**, 116476.
4 L. Wang, Q. Su, Y. Liu, T. Yimamumaimaiti, D. Hu, J.-J. Zhu and J.-R. Zhang, *Chem. Sci.*, 2022, **13**, 12136–12143.
5 P. Simons, S. A. Schenk, M. A. Gysel, L. F. Olbrich and J. L. M. Rupp, *Adv. Mater.*, 2022, **34**, 2109075.
6 P. Nithianandam, T. Liu, S. Chen, Y. Jia, Y. Dong, M. Saul, A. Tedeschi, W. Sun and J. Li, *Angew. Chem., Int. Ed.*, 2023, **62**, e202310245.
7 E. De la Paz, N. H. Maganti, A. Trifonov, I. Jeerapan, K. Mahato, L. Yin, T. Sonsa-Ard, N. Ma, W. Jung, R. Burns, A. Zarrinpar, J. Wang and P. P. Mercier, *Nat. Commun.*, 2022, **13**, 7405.
8 D. Maity, P. G. Ray, P. Buchmann, M. Mansouri and M. Fussenegger, *Adv. Mater.*, 2023, **35**, 2300890.
9 K. Veenuttranon, K. Kaewpradub and I. Jeerapan, *Nano-Micro Lett.*, 2023, **15**, 85.
10 H. Zhang, X. Sun, S. Hao and S. Dong, *Nano Energy*, 2022, **104**, 107940.
11 P. Zhao, X. Sun, S. Hao, Y. Zhang, J. Chen, H. Zhang and S. Dong, *ACS Energy Lett.*, 2023, **8**, 1697–1704.
12 L. Wang, H. Shao, X. Lu, W. Wang, J.-R. Zhang, R. Song and J.-J. Zhu, *Chem. Sci.*, 2018, **9**, 8482–8491.
13 C. H. Kwon, Y. Ko, D. Shin, M. Kwon, J. Park, W. K. Bae, S. W. Lee and J. Cho, *Nat. Commun.*, 2018, **9**, 4479.
14 Y. Huang, J. Ren and X. Qu, *Chem. Rev.*, 2019, **119**, 4357–4412.
15 S. He, L. Yang, P. Balasubramanian, S. Li, H. Peng, Y. Kuang, H. Deng and W. Chen, *J. Mater. Chem. A*, 2020, **8**, 25226–25234.
16 Z. Wang, R. Zhang, X. Yan and K. Fan, *Mater. Today*, 2020, **41**, 81–119.
17 Y. Jiang, T. Xia, L. Shen, J. Ma, H. Ma, T. Sun, F. Lv and N. Zhu, *ACS Catal.*, 2021, **11**, 2949–2955.
18 J. Chen, Q. Ma, M. Li, D. Chao, L. Huang, W. Wu, Y. Fang and S. Dong, *Nat. Commun.*, 2021, **12**, 3375.
19 M. Chu, Y. Zhang, L. Yang, Y. Tan, W. Deng, M. Ma, X. Su, Q. Xie and S. Yao, *Energy Environ. Sci.*, 2013, **6**, 3600–3604.
20 S. Qing, L. Wang, L. Jiang, X. Wu and J. J. Zhu, *SmartMat*, 2022, **3**, 298–310.
21 S. Zhao, P. Gai, W. Yu, H. Li and F. Li, *Chem. Commun.*, 2019, **55**, 1887–1890.
22 D. Tang, J. Liu, X. Zhang, L. Chen, L. Ma and Q. Zhang, *Green Chem.*, 2023, **25**, 7843–7862.
23 J. Zhao, H. Zhang, X. Sun, S. Hao, P. Zhao, X. Zhu and S. Dong, *J. Mater. Chem. A*, 2023, **11**, 600–608.
24 F. Pu, Y. Xiao, X. Yang, F. Yu, L. Xia, J. Chen, L. Wu, J. Xie, W. Zhao, Y. Liu, L. Wang, J. Ying, M. Liao, K. I. Ozoemena, G. Tian, F. Wang and X. Yang, *Chem. Eng. J.*, 2023, **474**, 145630.
25 L. Zhang, J. Zhu, X. Li, S. Mu, F. Verpoort, J. Xue, Z. Kou and J. Wang, *Interdiscip. Mater.*, 2023, **2**, 173–174.
26 H. Huo, Z. Xu, T. Zhang and C. Xu, *J. Mater. Chem. A*, 2015, **3**, 5882–5888.
27 M. Huang, C. Zhou, J. Tian, K. Yang, H. Yang and J. Lu, *Biosens. Bioelectron.*, 2020, **165**, 112357.
28 X. Feng, X. Feng and F. Zhang, *J. Mater. Chem. A*, 2023, **11**, 20242–20253.
29 T. W. Kim and K. S. Choi, *Science*, 2014, **343**, 990–994.
30 R. Chen, Y. Zhang, D. Wang and H. Dai, *J. Am. Chem. Soc.*, 2001, **123**, 3838–3839.
31 P. Cheng, H. Wang and X. Shi, *Nanoscale*, 2020, **12**, 3050–3057.
32 W. Liu, Z. Xu, D. Zhao, X. Pan, H. Li, X. Hu, Z. Fan, W. Wang, G. Zhao, S. Jin, G. W. Huber and H. Yu, *Nat. Commun.*, 2020, **11**, 265.
33 Z. Tian, Y. Da, M. Wang, X. Dou, X. Cui, J. Chen, R. Jiang, S. Xi, B. Cui, Y. Luo, H. Yang, Y. Long, Y. Xiao and W. Chen, *Nat. Commun.*, 2023, **14**, 142.
34 D. Guo, H.-F. Wei, X.-Y. Yu, Q. Xia, Z. Chen, J.-R. Zhang, R.-B. Song and J.-J. Zhu, *Nano Energy*, 2019, **57**, 94–100.